## Title

# Robust trigger wave speed in *Xenopus* cytoplasmic extracts

## Authors

Jo-Hsi Huang[1, 3], Yuping Chen[1, 3], William Y. C. Huang[1], Saman Tabatabaee[1], and James E. Ferrell Jr.[1, 2, 4]

1. Department of Chemical and Systems Biology, Stanford University School of Medicine, Stanford, CA 94305-5174, USA

2. Department of Biochemistry, Stanford University School of Medicine, Stanford, CA 94305-5307, USA

3. These authors contributed equally

4. Corresponding author

## Keywords

Cytoplasm; *Xenopus* egg extract; signal transduction; reaction-diffusion system; robustness; scaling relationship; molecular crowding; positive feedback loop; diffusion; rate coefficient

**ABSTRACT**

Self-regenerating trigger waves can spread rapidly through the crowded cytoplasm without diminishing in amplitude or speed, providing consistent, reliable, long-range communication. The macromolecular concentration of the cytoplasm varies in response to physiological and environmental fluctuations, raising the question of how or if trigger waves can robustly operate in the face of such fluctuations. Using *Xenopus* extracts, we found that mitotic and apoptotic trigger wave speeds are remarkably invariant. We derived a model that accounts for this robustness and for the eventual slowing at extremely high and low cytoplasmic concentrations. The model implies that the positive and negative effects of cytoplasmic concentration (increased reactant concentration vs. increased viscosity) are nearly precisely balanced. Accordingly, artificially maintaining a constant cytoplasmic viscosity during dilution abrogates this robustness. The robustness in trigger wave speeds may contribute to the reliability of the extremely rapid embryonic cell cycle.

[141 words]

## INTRODUCTION

Frog eggs are large cells that are particularly well-suited to quantitative biochemical studies. The eggs are about 1.3 mm in diameter and 1 µL in volume, which makes them amenable to single-cell biochemical assays[1]. Moreover, they can be lysed with minimal dilution, and the undiluted cytoplasm can be recovered and studied[2,3]. These egg extracts self-organize into cell-like compartments[4], and like the cells from which they are derived, they can carry out rapid cell cycles[2,5,6] and, under adverse conditions, die by apoptosis[7,8]. Indeed, *Xenopus* egg extracts have provided important insights into the regulation of both the cell cycle and apoptosis.

The large size of the frog egg presents a challenge shared by other large cells and tissues: how to coordinate rapid processes like mitotic entry and apoptotic death across such large distances. Early modeling work on the cell cycle suggested that mitosis might spread through the egg via trigger waves of Cdk1 activity[9]. Trigger waves can occur in systems with positive feedback loops, and they spread faster over large distances than diffusion alone would allow[10,11]. Experimental work has shown that mitosis does spread through *Xenopus* cytoplasm via trigger waves[5,12], at a speed of ~60 µm $min^{-1}$, and apoptosis does as well, at about half that speed[8]. A growing body of evidence suggests that trigger waves may be a common way of transmitting signals over large distances in biological systems. Action potentials and calcium waves are familiar examples of trigger waves, as are intercellular cAMP waves in swarming *Dictyostelium*[13–15] and intercellular ERK waves in wounded fish scales[16] and mouse skin[17]. Recent work suggests that the remarkable regeneration of an amputated planarian depends upon signals transmitted from the wound site via intercellular trigger waves of ERK activation[18].

The cytoplasm is a crowded, spatially organized mixture of organelles, macromolecules, and small molecules. Protein concentrations in *Xenopus* extracts[19–21] and mammalian cell lines[22] are typically on the order of 75 mg $mL^{-1}$, although it is higher in some cells, e.g. erythrocytes. It has been conjectured that the nominal cytoplasmic protein concentration maximizes the speed of important biochemical processes[23]. The extent to which this conjecture holds true for the cells awaits experimental investigations. Conversely, protein concentration is dynamic; it falls by

~15% when cells enter mitosis[24,25] and by ~50% when cells become senescent[26]. Cells change in volume when attaching to substrates of different stiffnesses[27,28], and recent work indicates that neutrophils swell by ~15% in response to chemoattractants, and that the swelling facilitates rapid migration[29]. The extent to which changes in volume, and changes in cytoplasmic concentration, impact the biochemistry of living cells is as yet poorly understood.

Here we ask how long-range communication via trigger waves is affected by changes in the concentration of cytoplasmic *Xenopus* egg extracts. We show that both mitotic and apoptotic trigger waves can be generated and propagated over a wide range of cytoplasmic concentrations. The wave speeds are maximal or near maximal at a 1x cytoplasmic concentration, in line with Dill's conjecture that the nominal 1x concentration maximizes the speeds of critical biochemical processes[21,23], and in the case of apoptotic trigger waves the speed is almost invariant over concentrations from 0.1x to 2x. We derive a simple general equation for trigger wave speed as a function of cytoplasmic concentration, which shows how balanced opposing effects are responsible for this robustness, and show that the equation satisfactorily accounts for our experimental observations. Finally, we show that disrupting the balance by maintaining a constant viscosity when diluting the extracts makes trigger wave speed highly sensitive to cytoplasmic concentration.

## RESULTS

### Mitotic trigger waves in concentrated and diluted extracts

Mitosis is brought about by a complex, interconnected regulatory system centered on a protein kinase, cyclin B-Cdk1, and two opposing phosphatases, PP1 and PP2A-B55 (Fig. 1a). Several positive feedback and double-negative feedback loops are embedded in this regulatory system; for example, active cyclin B-Cdk1 turns on its activator Cdc25, and cyclin B-Cdk1 and PP2A-B55 antagonize each other via intertwined double-negative feedback loops (Fig. 1a). The net result of these feedback loops is that the system functions as a bistable switch[30,31], and this bistability is key for the propagation of the mitotic state as a trigger wave[12].

To see how robust mitotic trigger waves are to changes in the concentration of the cytoplasm, we began by making either a 1x cytoplasmic extract or a concentrated extract on a Microcon spin column. From 4 independent preparations, the 1x cytoplasmic protein concentration was 57.9 ± 3.4 mg $mL^{-1}$ (mean ± S.E.M., n = 4; Fig. 1c), in line with other estimates[19–21], and not far from the protein concentrations measured for three common mammalian cell lines (~75 mg $mL^{-1}$)[22]. The concentrated extract was 116 ± 6.0 mg $mL^{-1}$ (mean ± S.E.M., n = 6; Fig. 1c); hereafter we will refer to it as a 2x retentate. The flow-through, which we will refer to as the filtrate, from the spin column had a protein concentration of less than 0.01 mg $mL^{-1}$ (Fig. 1c).

We then diluted the 1x extract or 2x retentate to various extents. In other recent work we used filtrate for the dilutions[21]. Here we have used XB buffer without sucrose rather than filtrate, which allowed us to produce larger volumes of diluted extracts, and we verified that the behaviors of the buffer-diluted and filtrate-diluted extracts were similar (Supplementary Fig. 1).

We added demembranated sperms and SiR-tubulin to the extracts and dilution buffers, made the dilutions, and aspirated extracts into ~100 µm or ~300 µm inside-diameter polytetrafluorethylene (PTFE) tubes under gentle vacuum. The tubes were placed under mineral oil and followed by fluorescence video microscopy. Fig. 1d, left panel, shows a typical result. At the first time point shown here, the extract was in interphase with stable microtubules throughout the length of the tube. Within a few minutes, mitosis began near the bottom of the tube and at a locus about 4 mm up the tube. As judged by the depolymerization of the fluorescent interphase microtubules, mitosis spread outward from these two loci in a linear fashion (Fig. 1d). Mitotic exit followed about 12 min after mitotic entrance, and it also spread linearly outward from the same two locations. Fig. 1d, right panel, shows the same data where instead of imaging the whole tube, we recorded SiR-tubulin fluorescence intensity along a line down the middle of the tube and then assembled the data into a kymograph. In either representation, the trigger wave character of mitotic propagation is apparent, and the speed of the mitotic front was 60.2 ± 3.2 µm $min^{-1}$ (mean ± S.E.M., n = 9), similar to previously reported mitotic wave speeds[5,12,32].

Next we examined how the cell cycle period and the speed of the mitotic waves were affected by changes in cytoplasmic concentration. Fig. 1e shows examples of kymographs from a diluted 1x extract and diluted 2x retentate. The periods of the first cycles and the wave speeds were calculated and are summarized in Figs. 1f and 1g, which include multiple experiments and more dilutions. Several general trends are apparent. First, the wave speeds were similar for 1x extracts and 2x retentates diluted back to 1x, but the periods were different, with the diluted 2x retentates having longer cell cycle periods than the corresponding 1x and diluted 1x extracts. Second, the cell cycle periods tended to be longer in diluted extracts than in concentrated extracts (Fig. 1f). Third, the diluted extracts tended to live longer than the concentrated extracts; a wave of apoptosis, which destroys the microtubule fluorescence, can be seen in the second and in fourth kymographs (Fig. 1e). Fourth, the most concentrated extracts tended to arrest in mitosis with depolymerized microtubules (Supplementary Fig. 2; cf. Fig. 1e, where the extract did not arrest in mitosis). And finally, the speeds of the mitotic waves were relatively invariant, with only the extracts at greater than 1x showing some slowing of the waves. Diluting the extract below 1x slightly increased the wave speed (by ~10%). For comparison, if the wave speed were determined by a bimolecular reaction, decreasing the extract from 1x to 0.5x might be expected to decrease the wave speed by 75%. Both the cell cycle frequency and mitotic wave speed were at or near their maximal values at 1x cytoplasmic concentration, consistent with Dill's conjecture[23].

**Apoptotic trigger waves in concentrated and diluted extracts**

Apoptosis is mediated by a complex system of regulators that bring about the activation of caspases 3 and 7, so-called executioner caspases that cleave diverse cellular proteins and bring a halt to the basic processes of life (Fig. 2a). There are several potential positive feedback loops in the apoptotic control system (Fig. 2a), raising the possibility that caspase activation could spread via trigger waves. In many cell types, apoptosis spreads through the cytoplasm in a wave-like manner[33–35], and in *Xenopus* egg extracts, where it is easy to obtain length scales over which the distinction between diffusive spread and trigger wave spread is unambiguous, it is clear that the fronts of caspase activation represent trigger waves that propagate without

slowing down or decreasing in amplitude[8]. The manipulability of extracts allowed us to assess the sensitivity of the apoptotic trigger wave speed in such extracts to cytoplasmic concentration, and to tease out the contributing effects quantitatively.

Interphase *Xenopus* egg extracts were prepared and were mixed with a rhodamine-based fluorogenic sensor of caspase 3/7 activation, $(Z\text{-}DEVD)_2$-R110, and a proteasome inhibitor (MG-132), which decreased the background level of R110 fluorescence and hence improved the signal-to-noise ratio of the experiment. The extracts were then loaded into thin (~100 µm diameter) PTFE tubes (Fig. 2b). Apoptosis was induced by briefly dipping one end of the tube into a reservoir of apoptotic extract, prepared by adding cytochrome c (2 µM) to fresh extract and incubating at room temperature for 30 min. The induced tubes were then immersed in heavy mineral oil in custom-made imaging chambers and imaged at 2 min intervals at room temperature.

Fig. 2b shows the results of a typical experiment. Apoptosis, as detected by bright R110 fluorescence, first initiated at the dipped end of the tube and then spread toward the other end. The propagation speed in this experiment was 29.6 µm $min^{-1}$; average speeds from 25 independent experiments were 27.5 ± 0.8 µm $min^{-1}$ (mean ± S.E.M.), This is similar to the speeds seen in the cycling extracts that underwent apoptosis in Fig. 1E (28.1 and 27.7 µm min-1) and agree well with previous reports[8].

We then altered the cytoplasmic concentration of the egg extract by diluting either a 1x extract or a 2x retentate. We verified apoptotic wave speed responds similarly to 3 different diluents (Supplementary Fig. 3) and chose XB buffer without sucrose as the primary diluent for further experiments. Fig. 2c shows kymographs of R110 fluorescence as a function of time for the original 1x extract and a 0.5x obtained by dilution, and for a 2x extract and a 1x extract reconstituted from the 2x extract by dilution; Fig. 2d shows data from 9 independent experiments, including additional extract concentrations. Overall, the apoptotic wave speed was almost invariant (Fig. 2d). There was no measurable change over a concentration range of

0.5x to 1x, and the speed decreased by only about 15% as the concentration increased to 2x (Fig. 2d). Thus, apoptotic wave speed is highly robust to variations in cytoplasmic concentration.

**Deriving an expression for wave speed as a function of cytoplasmic concentration**

To try to understand these trends, and in particular to understand how wave speed can be so insensitive to cytoplasmic concentration, we derived an expression for wave speed as a function of cytoplasmic concentration based on a simple model of a reaction-diffusion trigger wave system. We began by assuming that the complicated reaction schemes shown in Fig. 1a (for mitosis) and Fig. 2a (for apoptosis) can be approximated by simple one-species, bimolecular autocatalytic processes, as shown in Fig. 3a and in Eq. 1:

$$\frac{dC_{active}}{dt} = kC_{active}C_{inactive}, \qquad \text{[Eq 1]}$$

where $C_{active}$ denotes the concentration of active Cdk1 or caspase 3/7, $C_{inactive}$ is the concentration of inactive Cdk1 or caspase 3/7, and $k$ is a rate constant. We can eliminate one of the time-dependent variables by assuming that the total concentration of Cdk1 or caspase 3/7 is constant, and substituting as follows:

$$\frac{dC_{active}}{dt} = kC_{active}(C_{total} - C_{active}). \qquad \text{[Eq 2]}$$

This ordinary differential equation can be solved in closed form:

$$C_{active} = \frac{C_{total}}{1+\left(\frac{C_{total}-C_o}{C_o}\right)e^{-C_{total}kt}}, \qquad \text{[Eq 3]}$$

where $C_0$ is $C_{active}(t = 0)$. Eq. 3 is a logistic equation, identical in form to the equation that describes the growth of bacteria in the face of limited resources. The time course is a sigmoidal curve, where the steepness of the curve is determined by $C_{total}k$ and the time lag is determined by $C_{total}$, $C_0$, and $k$.

To test whether it was reasonable to be replacing the complicated reaction schemes for Cdk1 and caspase 3/7 control with the simple rate equation shown in Eq. 2, we asked whether Eq. 3 could be fitted to time course data for Cdk1 activation and caspase 3/7 activation in extracts. For Cdk1 activation (Fig. 3a), we made use of previously published data on the time course of Cdk1 activity, measured by H1 kinase assays, in *Xenopus* extracts[36]. As shown in Fig. 3b, the time course was well approximated by a logistic function until Cdk1 activity began dropping during late mitosis. Cdk1 activity fell after reaching its maximum because of the activation of the APC/C and the destruction of cyclins, which causes the cycling system to exit mitosis.

To measure the time course of caspase 3/7 activation, we encapsulated a mixture of 10% apoptotic extracts and 90% fresh interphase extract, plus (Z-DEVD)$_2$-R110, in squalene[37], and monitored the increase in R110 fluorescence as a function of time in individual droplets (10 – 100 µm diameter; Fig. 3c, d). The time course for one such droplet is shown in Fig. 3e. The time course of caspase 3/7 activation could be inferred by assuming irreversible production of R110 fluorescence by active caspase 3/7 and a nonspecific background process. As shown in Fig. 3f, the time course was well-approximated by a logistic function. Estimated caspase activities fell after reaching the maximum due to depletion of the fluorogenic substrate.

The fact that the logistic function describes the early time course justifies the use of Eq. 2 to replace the complex, multivariable reactions of the full system. This makes our reaction-diffusion model equivalent to the Fisher-Kolmogorov-Petrovsky-Piskunov (FKPP) model[38,39], which was originally formulated to describe the spreading of favorable genetic alleles through a population in space and time. For the one-dimensional case of trigger wave propagation in a thin tube, the resulting equation is:

$$\frac{dC_{active}}{dt} = D\frac{d^2C_{active}}{dx^2} + kC_{active}(C_{total} - C_{active}), \qquad \text{[Eq 4]}$$

where $D$ is the diffusion coefficient for the autocatalytic species.

In the FKPP model, the minimum speed of propagation, which is the trigger wave speed, is given by:

$$v = 2\sqrt{kC_{total}D}. \quad \text{[Eq 5]}$$

This is equivalent to Luther's equation, proposed in 1906 to account for the speed of chemical waves[40,41].

Note that all three of the variables under the square root sign might vary with the overall cytoplasmic concentration $\phi$. This can be expressed as:

$$v(\phi) = 2\sqrt{k(\phi)C_{total}(\phi)D(\phi)} \quad \text{[Eq 6]}$$

We assume $C_{total}(\phi)$ is simply proportional to the overall cytoplasmic concentration $\phi$:

$$C_{total}(\phi) = \phi C_1, \quad \text{[Eq 7]}$$

where $C_1$ denotes total caspase 3/7 or Cdk1 concentration at 1x cytoplasmic concentration. This assumption leaves two functions, $D(\phi)$ and $k(\phi)$, to be experimentally determined.

For mitotic trigger waves, likely mediators of the spatial spread include cyclin B-Cdk1, Cdc25, and Gwl, proteins with molecular weights of ~100 kDa. For apoptosis, plausible mediators include activated caspase 3 and 7 heterotetramers (~60 kDa) and cytochrome c (12 kDa). Therefore, we chose a similarly-sized probe, Alexa Fluor 488-labeled bovine serum albumin (AF488-BSA; ~67 kDa), for diffusion measurements. We measured its diffusion coefficient as a function of cytoplasmic concentration by fluorescence correlation spectroscopy (FCS). The diffusion mode of AF488-BSA was fairly close to Brownian in XB buffer without sucrose ($\alpha \approx 0.9$) and more subdiffusive in extracts ($\alpha \leq 0.8$; Fig. 4a, Supplementary Fig. 4). These observations are consistent with previous reports[42–45]. The effective diffusion coefficient

$D_{eff}(\phi)$, which is calculated assuming Brownian motion rather than subdiffusive motion, decreased exponentially with cytoplasmic concentration (Fig. 4b) ($R^2$ = 0.953), as predicted by Phillies' law[46,47]. The fitted effective diffusion coefficients in XB buffer without sucrose ($\phi = 0$) and 1x extract ($\phi = 1$) were 32 and 15 μm$^2$ s$^{-1}$ (Fig. 3b), respectively, again consistent with previous measurements[42]. We can therefore express the scaling of the effective diffusion coefficient $D_{eff}(\phi)$ as:

$$D_{eff}(\phi) = D_0 e^{-g_D \phi} \quad \text{[Eq 8]}$$

where $D_0$ is $D_{eff}(0)$ and $g_D$ is a dimensionless scaling factor with a fitted value of 0.765.

The remaining contributor to Eq 6 is $k(\phi)$, the rate constant for the bimolecular autocatalysis reaction. We do not have a good way of experimentally assessing this parameter for Cdk1 activation, since we are inferring Cdk1 activity indirectly from microtubule polymerization, but the more direct probes for caspase activation allow this relationship to be determined. To infer enzyme activities from fluorescence data, we first constructed an ordinary differential equation (ODE) model for how (Z-DEVD)$_2$-R110 dynamics depend upon caspase activity. We assumed that fluorescent rhodamine 110, designated $R$, is produced by caspase 3/7 and degraded by some unspecified enzyme, and that both production and degradation are approximated by mass action kinetics:

$$\frac{dR}{dt} = k_R C(R_{total} - R) + k_{BG}(R_{total} - R). \quad \text{[Eq 9]}$$

Here $R_{total}$ is the total concentration of (Z-DEVD)$_2$-R110 and its fluorescent product R110, $k_R$ the rate constant for caspase 3/7 cleaving (Z-DEVD)$_2$-R110, and $k_{BG}$ is the first-order rate coefficient for background/nonspecific production of R110. Eq 9 can be solved to obtain an expression for $R(t)$:

$$R(t) = R_{total} - (R_{total} - R_0)\left(\frac{C_0}{C_{total}}(e^{k_C C_{total} t} - 1) + 1\right)^{-\frac{k_R}{k_C}} e^{-k_{BG} t}, \quad \text{[Eq 10]}$$

with $R_0$ representing the fluorescent rhodamine 110 concentration and $C_0$ the concentration of the apoptotic mediator at $t = 0$. For clarity, we use $k_C$ to represent the bimolecular rate constant for caspase 3/7 autocatalysis, making it equivalent to $k$ in Eqs 4, 5, and 6.

There are 4 adjustable parameters in Eq 10; namely, $k_C$, $C_0$, $k_R$, and $k_{BG}$. We experimentally determined $k_R$ as a function of cytoplasmic concentration (Supplementary Fig. 5), thereby eliminating one adjustable parameter from Eq 10. We then experimentally measured the rate constant $k_C$ for the cleavage of (Z-DEVD)$_2$-R110 by caspase 3/7 in *Xenopus* egg extracts by quantifying the sensor cleavage as a function of time at each point in the tube, aligning the time courses, and fitting the model to the aligned traces (Fig. 4d). This procedure was then repeated for various cytoplasmic concentrations.

One might expect $k_C(\phi)$ to be roughly constant since most enzymes operate far from the calculated Smoluchowski limit for diffusion control. However, $k_C(\phi)$ decreased exponentially with increasing cytoplasmic concentration ($R^2$ = 0.901; Fig. 4e). We can therefore express the scaling of $k_C(\phi)$ as:

$$k_C(\phi) = k_0 e^{-g_k \phi} \quad \text{[Eq 11]}$$

where $k_0 \equiv k_C(\phi = 0)$ and $g_k$ is the scaling factor, which were empirically estimated to be of 0.0022 nM$^{-1}$ min$^{-1}$ and 0.531, respectively. We can then rewrite Luther's equation to explicitly include the three concentration dependencies:

$$v(\phi) = 2\sqrt{k_0 C_1 D_0 \phi e^{-(g_k + g_D)\phi}} \quad \text{[Eq 12]}$$

We can further simplify Eq 12 by defining:

$$A \equiv k_0 C_1 D_0$$

$$g \equiv g_k + g_D$$

and arrive at the following expression:

$$v(\phi) = 2\sqrt{A\phi e^{-g\phi}} \qquad \text{[Eq 13]}$$

where $A$, the speed factor, determines the magnitude of the trigger wave speed, and $g$, the cytoplasmic concentration scaling factor, determines how steeply the speed decreases at high cytoplasmic concentration. Using $A$ and $g$ as adjustable parameters, Eq 13 fits well to the experimental data for apoptotic wave (Fig. 5a). We can also compare the fitted parameters to the quantities that contribute to them as estimated by experiments. Both $g_k$ and $g_D$ were individually measured (Fig. 4b, f), and their sum is close to the fitted value of $g$ (Fig. 5b). The product of the experimentally estimated values of $k_0$, $C_1$, and $D_0$ was also in reasonable agreement with the fitted value (Fig. 5b). The agreement between the directly measured values for these parameters and the values inferred from the trigger wave speed measurements is reassuring.

Note that Eq 13 also predicts that at low cytoplasmic concentrations the wave speed should decrease, a trend that was not apparent in the initial experimental data (Fig. 5a). To test this prediction, we repeated the experiment over very low cytoplasmic concentrations, and, as shown in Fig. 5c, the low concentration data agreed well with curve fitting carried out on the higher concentration (0.5x to 2x) results alone. Taken together, these findings show that combining the FKPP expression for trigger wave speed and Phillies' equation for the concentration dependence of diffusion-limited enzyme activities yields an equation that accounts for the dependence of trigger wave speed on cytoplasmic concentration, including the near-maximal speed at 1x concentration, the robustness of the trigger wave speed over a wide

range of cytoplasmic concentrations, and the fall-off in speed at very high and very low concentrations.

Eq 13 could also be fitted well to the mitotic wave speed data (Fig. 5d). The fitted $g$ value was larger (1.54 vs. 1.34), which accounts for the observation that the wave speed fell more steeply with increasing cytoplasmic concentration.

**Mechanism of the robust apoptotic trigger wave speed**

The robustness of the trigger wave speed appears to arise because one factor that influences wave speed, the concentration of the diffusible apoptotic mediator $C_{total}$, increases with increasing cytoplasmic concentration, whereas the autocatalytic rate constant $k_C$ and diffusivity $D_{eff}$ decrease. Perfect robustness would arise if the competing trends canceled exactly. Here we examine in more detail how close to exact the cancelation is and why it breaks down at very high and very low cytoplasmic concentrations.

We first expressed these functions in relative terms:

$$v_{rel}(\phi) \equiv \frac{v(\phi)}{v(\phi=1)},$$
$$C_{rel}(\phi) \equiv \frac{C_{total}(\phi)}{C_{total}(\phi=1)},$$
$$k_{rel}(\phi) \equiv \frac{k_C(\phi)}{k_C(\phi=1)},$$
$$D_{rel}(\phi) \equiv \frac{D_{eff}(\phi)}{D_{eff}(\phi=1)}.$$

Defining these relative quantities allows us to focus on the dependencies on cytoplasmic concentration $\phi$ while the proportionality constants $C_1$, $k_0$, and $D_0$ cancel out. We can also express Eq 6 in relative terms:

$$v_{rel}(\phi) = \sqrt{k_{rel}(\phi) C_{rel}(\phi) D_{rel}(\phi)}, \qquad \text{[Eq 14]}$$

If we take the logarithm, then the individual factors combine additively rather than multiplicatively:

$$\log v_{rel}(\phi) = \frac{1}{2}(\log k_{rel}(\phi) + \log C_{rel}(\phi) + \log D_{rel}(\phi)), \quad \text{[Eq 15]}$$

A robust trigger wave speed means $v_{rel}(\phi)$ should be close to 1 for a range of cytoplasmic concentration $\phi$. With log-transformation applied, a robust speed should have $\log v_{rel}(\phi)$ close to 0, meaning that the right-hand side of Eq 15 should also be close to 0:

$$\log k_{rel}(\phi) + \log C_{rel}(\phi) + \log D_{rel}(\phi) \approx 0. \quad \text{[Eq 16]}$$

From 0.5x to 1x cytoplasmic concentration, the decrease in $\log D_{rel}(\phi)$ and $\log k_{rel}(\phi)$ combined (blue and green bars, respectively) is nearly equal to the gain in $\log C_{rel}(\phi)$ (red bars, plotted as negative to aid visual comparison; Fig. 6a). This explains why the apoptotic wave speed is almost constant over that range of concentrations. At higher cytoplasmic concentrations, the negative factors ($\log D_{rel}(\phi)$ and $\log k_{rel}(\phi)$) are larger in magnitude than the positive factor ($\log C_{rel}(\phi)$), and so the wave speed decreases with increasing cytoplasmic concentration, and at very low cytoplasmic concentrations, the opposite is true (Fig. 6a). Thus, the robustness of the trigger wave speed arises from the precise balancing of opposing kinetic and biophysical quantities over a range of cytoplasmic concentrations.

**Artificially maintaining diffusivity abrogates trigger wave speed robustness**

One strong prediction is that if we could dilute an extract without increasing its diffusivity, the robustness of the trigger wave speed would be compromised. Toward this end we tested two viscogens, sucrose and BSA, and determined what concentrations would yield buffer solutions with diffusion coefficients equal to those seen in 1x cytoplasm. Using FCS and AF488-BSA, we found that 0.8 M sucrose (Fig. 6b) and 150 mg $mL^{-1}$ BSA (Fig. 6e) yielded diffusivities equivalent to that of 1x cytoplasm. We then diluted 1x cytoplasmic extracts with these buffers and asked whether trigger wave speed was no longer robustly maintained. As shown in Fig. 6c, f, trigger

wave speed was now dependent upon cytoplasmic concentration over this range. Intermediate concentrations of the viscogens yielded intermediate wave speed results (Fig. 6d, g). Thus the exact balancing of the effects of cytoplasmic diffusivity and reactant concentration is the basis for the robustness in trigger wave speed.

## DISCUSSION

### The robustness of trigger wave speeds

Over the past several years it has become increasing clear that trigger waves are a recurring theme in both intracellular[8,12] and intercellular[13–18] communication. Unlike diffusive spread, trigger waves allow signals to propagate without diminishing in amplitude or slowing in speed. Trigger waves are complex, systems-level phenomena; they require biological reactions that include positive feedback loops, plus a spatial coupling mechanism. Any system as complicated as this is bound to have vulnerabilities. Here we have examined how vulnerable two intracellular trigger waves, apoptotic waves and mitotic waves, are to variation in the cytoplasmic concentration, a basic cellular property that differs from cell type to cell type, and even varies in individual cells as they proceed through mitosis. We found that even though a priori one might expect that a bimolecular reaction's speed would vary as the square of the cytoplasmic concentration, both apoptotic and mitotic wave speeds were nearly constant when extracts were diluted down from 1x to lower concentrations, and fell modestly at higher-than-physiological concentrations. We derived a simple model that accounts for both the robustness of trigger wave speed and the slowing seen at very high and very low cytoplasmic concentrations. The model implies that the robustness arises from canceling effects of cytoplasmic concentration: increasing cytoplasmic concentration should increase the speed by increasing the concentrations of the reactants, but should also decrease the speed by increasing viscosity and hence slowing both the local coupling process (diffusion) and the rate constants for the positive feedback reactions. This implies that if one were to change cytoplasmic concentration without changing viscosity, by diluting cytoplasm with buffer supplemented with the appropriate concentration of a viscogen, the wave speed should cease to be invariant, and indeed this was found to be the case. For large cells, such as the *Xenopus*

eggs, the robustness of the mitotic wave speed could contribute to the reliability of the extremely rapid embryonic cell cycles in face of the physical stresses expected when an oocyte proceeds from the isotonic environment of the ovary to the hypotonic environment of the pond.

As mentioned above, recently it has been shown that some biological signals propagate as intercellular trigger waves in cell culture and in living tissues. Our theoretical framework may apply to tissue-level signal relay with appropriate generalization, with an intercellular process taking the place of intracellular diffusion as the local coupling mechanism.

This work adds to our burgeoning understanding of how physical properties of the cytoplasm constrain the operation of fundamental cellular processes. The present work also highlights the power of the *Xenopus* egg extract for studying the emergent regulatory functions that come from the differential responses of complex, coupled physical and biochemical processes.

**Limitations of the study**

We relied on several approximations to access the analytical power of Luther's and FKPP equations. Experimentally, we approximated diffusivity for caspase 3/7 and mitotic machines (CDK1/CycB and PP2A/B55 complexes) with AF488-BSA. Based on size, we may slightly over- or underestimate the scaling factor $g_D$, respectively. For diffusivity, we approximated anomalous diffusion with effective Brownian diffusion at a short distance range. Depending on the true length scale of diffusive mixing in trigger wave propagation, we may slightly over- or underestimate protein mobility. Model-wise, we approximated the overcoming of bistable switches (both mitotic and apoptotic onset are considered bistable transitions) as logistic growth processes. We may slightly underestimate the true rate coefficient depending on the true magnitude of ultrasensitivity. By adopting a combined positive feedback loop approach, we were not able to resolve the exact steps at which apoptosis or mitosis are limited by molecular crowding. Despite these limitations, our prediction error for apoptotic trigger wave speed was around 20% from the measured values, suggesting a good overall approximation.

466 Better experimental approximation and further developments in the theoretical treatments for
467 anomalous diffusion and traveling waves in bistable media should improve the prediction
468 accuracy and provide more detailed understandings to this topic.
469

470 **METHODS**

471 **Key resource table**

| **Chemicals, Peptides, and Recombinant Proteins** | **Source** | **Identifier** |
|---|---|---|
| Pregnant mare serum gonadotropin | Fisher Scientific | 50-893-505 |
| Chorionic gonadotropin human | Sigma | CG10-10VL |
| L-cysteine | Sigma | 168149 |
| A23187 | Sigma | C7522 |
| Leupeptin | Sigma | L2023 |
| Chymostatin | Sigma | C7268 |
| Pepstatin A | Sigma | P5318 |
| Cytochalasin B | Sigma | C6762 |
| MG-132 | Selleckchem | S2619 |
| Cycloheximide | Sigma | 01810 |
| cOmplete protease inhibitor cocktail, EDTA-free | Sigma | 5892953001 |
| Sucrose | Sigma | S8501 |
| Bovine serum albumin | Sigma | A3294 |
| SiR-Tubulin | Cytoskeleton, Inc. | CY-SC002 |
| $(Z\text{-}DEVD)_2$-R110 | AAT Bioquest | 13430 |
| Alexa Fluor 488 labeled bovine serum albumin | Thermo Fisher | A13100 |
| Cytochrome c purified from equine heart | Sigma | C2867 |
| **Experimental model: Organisms/strains** | **Source** | **Identifier** |
| *Xenopus laevis* females and eggs | NASCO | LM00531 |
| *Xenopus laevis* males and sperms | NASCO | LM00715 |
| **Reagents and materials** | | |
| Mineral oil, heavy | Sigma | 330760 |
| PTFE tubes | Cole Parmer | EW-06417-72 |

| | | |
|---|---|---|
| 10 kDa molecular weight cut-off filter | Sigma | UFC501096 |
| Bio-Rad protein assay dye concentrate | Bio-Rad | 5000006 |
| SimplyBlue SafeStain | Thermo Fisher | LC6065 |
| **Software and Algorithms** | **Source** | **Identifier** |
| ZEN | Zeiss | N/A |
| Igor Pro, version 6 | WaveMetrics | https://www.wavemetrics.com/ |
| FIJI / ImageJ, | FIJI | https://imagej.net/software/fiji/ |
| R, version 4.0.2 | The R project | https://www.r-project.org/ |
| SAEMIX | CRAN | https://cran.r-project.org/web/packages/saemix/index.html |
| Mathematica, version 13.2 | Wolfram Research | https://www.wolfram.com/mathematica/ |

## Resource availability

### Lead contact

Further information and requests for resources and reagents should be directed to and will be fulfilled by the lead contact.

### Material availability

Materials used in this study will be made available upon request.

### Data and code availability

Datasets and custom-written codes generated in this study will be made available upon request.

## Experimental model and subject details

### *Xenopus laevis*

The animal work adhered to relevant national and international guidelines and received approval from the Stanford University Administrative Panel on Laboratory Animal Care (APLAC protocol 13307). *Xenopus laevis* females, aged over 3 years, were prepared by dorsal cavity injection of 100 U of pregnant mare serum gonadotropin (PMSG) at least 3 days prior to, but typically no more than 2 weeks before ovulation. Ovulation was induced through dorsal cavity

injection of 200 U of human chorionic gonadotropin (hCG). These induced females were then housed in separate chambers containing egg-laying buffer (100 mM NaCl, 2 mM KCl, 1 mM $MgSO_4$, 2.5 mM $CaCl_2$, 500 µM HEPES, 100 µM EDTA, pH 7.4).

**Preparation of demembranted *Xenopus* sperm chromatin**

Demembranated *Xenopus laevis* sperm chromatin was prepared as described by Murray[48]. Typical experiments with cycling extracts included sperm nuclei, which serve as pacemakers for mitotic waves, at ~100 nuclei per µL extract.

**Preparation of *Xenopus* egg extracts**

We followed previously established procedures[49] to prepare *Xenopus* egg extracts with slight adaptations. Specifically, eggs were collected approximately 22 hours post hCG injection, selecting high-quality eggs with consistent pigment distribution and a well-defined white spot on the animal pole. The jelly coats were removed by incubation with dejellying buffer (20 mg $mL^{-1}$ L-cysteine, pH 7.8) for no more than 5 min. Subsequently, the eggs underwent a minimum of three washes in 0.2× Marc's modified Ringer's solution (0.2× MMR; 20 mM NaCl, 400 µM KCl, 400 µM $CaCl_2$, 200 µM $MgCl_2$, 1 mM HEPES, 20 µM EDTA, pH 7.8).

For cycling extracts, the eggs were activated with calcium ionophore A23187 (0.5 µg $mL^{-1}$) in 0.2× MMR prior to packing and crushing. The A23187-containing buffer was promptly removed upon egg activation, generally within 2 min, determined by the contraction of the animal pole. In the case of interphase-arrested extract, the activation step was omitted. After activation, the eggs were thoroughly washed with crushing buffer (50 mM sucrose, 100 mM KCl, 100 µM $CaCl_2$, 1 mM $MgCl_2$, 10 mM HEPES-KOH, pH 7.7) at least twice before packing through low-speed centrifugation (200 *g* for 1 minute, followed by 600 *g* for 30 s). After packing, care was taken to remove excess crushing buffer above the eggs to minimize dilution. Importantly, for cycling extracts, we waited at least 20 min post-activation to ensure meiotic exit was completed before transferring the packed eggs to ice, followed by subsequent centrifugation.

519 The eggs were subsequently crushed using a centrifugal force of 16,000 *g* at 4°C for 15
520 min. The resulting cytoplasmic fraction was collected as *Xenopus* egg extract and kept on ice.
521 Peptidase inhibitor mix (10 µg $mL^{-1}$ leupeptin, 10 µg $mL^{-1}$ pepstatin, 10 µg $mL^{-1}$ chymostatin)
522 and actin polymerization inhibitor cytochalasin B (10 µg $mL^{-1}$) were added into the extract. In
523 the case of interphase-arrested extract, cycloheximide (CHX; 100 µg $mL^{-1}$) was included to
524 prevent cyclin B translation and, thus, entry into mitosis. CHX was excluded from cycling
525 extracts. The extracts underwent one or two additional rounds of centrifugation at 16,000 *g* at
526 4°C for 5 min to eliminate impurities before further use.
527
528 **Dilution, concentration, and reconstitution of *Xenopus* egg extracts**
529 We used XB buffer without sucrose (100 mM KCl, 100 µM $CaCl_2$, 1 mM $MgCl_2$, 10 mM HEPES-
530 KOH, pH 7.7) as the primary diluent for adjusting cytoplasmic concentration. In experiments
531 involving viscogens, sucrose or BSA were titrated in XB buffer without sucrose to the required
532 concentrations from stocks with the same salt content as the basal XB buffer. We concentrated
533 the extracts using a 10 kDa molecular weight cut-off centrifugal filter. We could achieve a 2-fold
534 concentration by centrifuging three times for 10 min at 4°C (a total of 30 min), homogenizing
535 the extracts between each spin with gentle pipetting. Dilution and reconstitution were carried
536 out by mixing extracts with the appropriate diluents to reach the desired volume fraction.
537
538 **Determination of protein concentration**
539 Protein concentration was determined using the Bio-Rad protein assay, a method based on the
540 Bradford assay. Briefly, undiluted extract was first diluted 200-fold in XB buffer without sucrose
541 and then quantified in accordance with the manufacturer's instructions, measuring absorbance
542 at 595 nm. The retentate was first diluted two-fold and quantified in the same manner as the
543 undiluted extract. We also determined the protein concentration in the filtrate (flow-through)
544 during the concentration process. The filtrate was directly assessed using the Bio-Rad assay,
545 without additional dilution or processing.
546
547 **Measurements of apoptotic and mitotic trigger wave speeds**

**Experimental setup**

To monitor apoptotic and mitotic trigger waves, we mixed extracts with biosensors and filled PTFE tubes (~100 µm inner diameter) for subsequent time-lapse fluorescent microscopy. We used interphase-arrested extracts for apoptotic trigger wave propagation. Caspase 3/7 activity was monitored using $(Z\text{-}DEVD)_2$-R110 at 2 µM, unless otherwise specified. To enhance the signal-to-noise ratio, we included 200 µM MG-132 to inhibit the proteasomal cleavage of $(Z\text{-}DEVD)_2$-R110. Following tube filling, we let the extract-filled tubes stand at room temperature for 30 min before inducing apoptosis. Apoptosis was initiated by briefly dipping the tube end into a reservoir of apoptotic extract, which was prepared by adding 2 µM cytochrome c to fresh extract and incubating at room temperature for 30 min. The induced tubes were placed in custom-made imaging chambers, submerged in heavy mineral oil, and imaged at 2-min intervals at room temperature.

To monitor mitotic trigger waves, cycling extracts were used. We tracked the dissolution of microtubules during mitosis as an indicator of mitotic activity, with SiR-tubulin (200 nM) serving to visualize polymerized microtubules. Following the filling of PTFE tubes (~100 or ~300 µm in diameter), the tubes were immersed in heavy mineral oil within custom-made imaging chambers and imaged at 2 to 3-minute intervals at room temperature.

For each cytoplasmic concentration, we typically had several biological replicates (independent samples), which involved extracts prepared from different clutches of eggs obtained from different females. Within each biological replicate, several tubes (up to 5) were monitored as technical replicates. Typically, 1 to 2 waves per technical replicate were observed for apoptotic wave experiments, while more than 2 waves per technical replicate were typical for mitotic wave experiments.

**Measurement of wave speeds from kymographs**

Kymographs were constructed from time-lapse videos capturing the propagation of trigger waves within PTFE tubes using Multi Kymograph in FIJI/ImageJ, with the width parameter set to 3 pixels. The dimensions and signal intensity of the kymographs were adjusted to optimize visual inspection. To facilitate speed measurements of mitotic waves, we increased the contrast

577 of the SiR-tubulin signal for better visualization. For apoptotic waves, images were binarized
578 with a consistent signal cut-off by applying a unique global signal threshold to each image.
579 Subsequently, straight lines were manually fitted to the linear segments of the propagating
580 waves, and wave speed was determined from the slopes of these fitted lines.

581 Each biological replicate (independent sample) included up to 5 tubes as technical
582 replicates. A median speed was initially calculated for each tube (tube median), followed by the
583 determination of a median speed for a given biological replicate (biological replicate median)
584 from the tube medians. Means and S.E.M. for each condition were then computed from the
585 biological replicate medians.

586

587 **Measurement of protein diffusivity by FCS in *Xenopus* egg extract**

588 FCS measurements in *Xenopus* egg extract were analyzed following a previously described
589 method[42]. In brief, interphase-arrested extracts were prepared, and cytoplasmic concentration
590 was adjusted as mentioned earlier. We included the EDTA-free cOmplete protease inhibitor
591 cocktail at a 1:50 (v/v) ratio, 30 min prior to the addition of 25 nM Alexa Fluor 488 labeled BSA
592 (AF488-BSA) to the extracts. FCS data were acquired using an inverted Zeiss LSM 780
593 multiphoton laser scanning confocal microscope at room temperature (22°C). The microscope
594 setup and the calibration step were described previously[42].

595 The confocal spot was focused 30 – 40 µm above the dish surface. Each data point
596 represented the average of at least 3 randomly selected positions within the extract field. At
597 each position, fluorescence intensities were acquired for 60 s. Autocorrelation functions were
598 calculated directly by the ZEN 2.3 SP1 FP3 310 (Black) software (version 14) (Zeiss) controlling the
599 microscope. An anomalous diffusion model or a Brownian diffusion model were used to fit the
600 autocorrelation functions:

601

602 $$G(\tau) = \frac{1}{N\left(1+\left(\frac{\tau}{\tau_D}\right)^{\alpha}\right)\sqrt{\left(1+\frac{1}{s^2}\left(\frac{\tau}{\tau_D}\right)^{\alpha}\right)}}, \qquad \text{[Eq S1]}$$

603

where $G(\tau)$ denotes the autocorrelation function, $\alpha$ signifies the diffusion-mode parameter as defined by the mean squared displacement (MSD) equation $MSD(t) \propto t^{\alpha}$, $\tau_D$ represents the characteristic diffusion time, $N$ corresponds to the particle number, and $s$ stands for the structural parameter of the optics. The Brownian diffusion model is identical to the anomalous model except for the $\alpha$ value, which is set to 1.

Consistent with prior reports[42], protein diffusion in *Xenopus* egg extract displayed weakly subdiffusive behavior, akin to cultured mammalian cells, and was better described by the anomalous diffusion model. Nevertheless, an effective diffusion coefficient can be calculated from $D_{eff} = \langle r^2 \rangle / (4\tau_D)$ where $r$ is the radius of the confocal spotsize.

## Logistic dynamics approximation of mitotic and apoptotic activities

### CDK1 activity in cycling *Xenopus* egg extract

Measurements of CDK1 activity in the cycling *Xenopus* egg extract were made previously by Pomerening et al[36]. We focused on data points corresponding to the onset and exit of mitosis (60 to 90 min). The relative CDK1 activity was renormalized, and a logistic curve was fitted to the data within the selected time range up to the point when maximal activity was reached.

### Caspase 3/7 activation in encapsulated extract droplets

For encapsulating interphase extract in oil, we followed the method outlined by Good and Heald[37]. In brief, we mixed 10% (v/v) apoptotic extract with fresh extract to induce the onset of apoptosis. Additionally, we included 10 µM $(Z\text{-}DEVD)_2$-R110 to monitor caspase 3/7 activity. A low concentration of TexasRed-labeled dextran was added as a soluble marker for extract volume during image analysis. Subsequently, we added 1:20 volume of extract into squalene supplemented with 5% (v/v) Cithrol DPHS-SO-(AP) and agitated the tube with force to create an emulsion of encapsulated extract droplets. These droplets were then imaged at 10-second intervals using an epifluorescence microscope. The increase in fluorescence in the droplets was individually tracked using ImageJ.

We estimated active caspase 3/7 concentration over time by employing a set of ordinary differential equations (ODEs) as described in the main text (Eqs 2, 3, 9, and 10; see

633 below). Essentially, caspase 3/7 activation was analyzed as an irreversible, bimolecular reaction
634 following mass action principles. The cleavage of (Z-DEVD)$_2$-R110 by caspase 3/7 was similarly
635 modeled as an irreversible, bimolecular reaction based on mass action principles, while its
636 nonspecific background cleavage in the extract was represented as an irreversible, first-order
637 reaction following mass action.
638
639 **Estimation of caspase 3/7 activation rate coefficient**
640 **Model for caspase 3/7 activation and (Z-DEVD)$_2$-R110 cleavage**
641 We deduced caspase 3/7 activation kinetics from the cleavage kinetics of (Z-DEVD)2-R110. To
642 do this, we constructed a simple model with two ordinary differential equations (ODEs) based
643 on two key approximations. First, we approximated caspase 3/7 activation kinetics with logistic
644 growth. Second, we approximated caspase 3/7 activation and (Z-DEVD)2-R110 cleavage at the
645 pixel resolution using the following ODE:
646

647 $$\frac{dC}{dt} = k_C C(C_{total} - C). \qquad \text{[Eq S2]}$$

648
649 Here, $C$ denotes concentration of active caspase 3/7, $C_{Total}$ the total concentration of inactive
650 and active caspase 3/7, and $k_C$ the rate coefficient for the activation of caspase 3/7 through
651 positive feedback. Logistic growth can be described in the following closed-form expression:
652

653 $$C(t) = \frac{C_{total}C_0}{C_0 + (C_{total} - C_0)e^{-k_C C_{total} t}}, \qquad \text{[Eq S3]}$$

654
655 where $C_0$ denotes caspase 3/7 concentration at $t = 0$. Activated caspase 3/7 and nonspecific
656 background activity consume (Z-DEVD)$_2$-R110 and release fluorescent rhodamine 110 (R110):
657

658 $$\frac{dR}{dt} = k_R C(R_{total} - R) + k_{BG}(R_{total} - R), \qquad \text{[Eq S4]}$$

659

Here $R$ denotes free, fluorescent R110, $R_{total}$ the total concentration of (Z-DEVD)$_2$-R110 and R110, $k_R$ the rate coefficient of caspase 3/7 cleaving (Z-DEVD)$_2$-R110, and $k_{BG}$ the first-order rate coefficient of background cleavage. To reduce the number of fitting parameters in the equation, we experimentally determined $k_R$ for cytoplasmic concentration ranging from 0.5x to 2x (see below). We found a solution to $R(t)$:

$$R(t) = R_{total} - (R_{total} - R_0)\left(\frac{C_0}{C_{total}}(e^{k_C C_{total} t} - 1) + 1\right)^{-\frac{k_R}{k_C}} e^{-k_{BG} t}, \qquad \text{[Eq S5]}$$

with $R_0$ representing fluorescent R110 concentration at $t = 0$.

**Determination of the apparent (Z-DEVD)$_2$-R110 cleavage rate coefficient**

We measured (Z-DEVD)$_2$-R110 cleavage rate in freshly prepared, fully apoptotic extracts. Briefly, apoptosis was induced by introducing 2 μM cytochrome c to interphase extracts and incubated for 30 min at room temperature to fully activate caspase 3/7. Subsequently, 5 μM (Z-DEVD)$_2$-R110 was introduced to the apoptotic extracts, mixed vigorously by high-speed vortex, and the fluorescence increase was promptly recorded. Maximal cleavage rates were determined from the initial time points using linear fitting ($R^2 \geq 0.99$). The apparent second-order rate coefficients were then calculated from these maximal rates.

We made two assumptions. First, we assumed that caspase 3/7 concentration is linearly proportional to the overall cytoplasmic concentration and is 200 nM in 1x extracts. Second, we assumed a negligible decrease in (Z-DEVD)$_2$-R110 during the early time points.

**Estimation of (Z-DEVD)$_2$-R110 cleavage kinetics from image brightness**

The same kymographs employed for trigger wave speed measurements were utilized here. Signals were scaled, and the signal intensity was subsequently correlated with the nominal concentration of R110. To estimate the signal intensity asymptote, we employed a two-component Gaussian mixture model on the kymograph, with the larger component conveniently providing an estimate of the asymptote. Subsequently, we subtracted the background intensity and adjusted the signal accordingly. The signal intensity at $t = 0$,

therefore, also provided an estimate of $R_0$, the initial rhodamine 110 concentration, reducing the parameters to be fitted to just three: $C_0$, $k_C$, and $k_{BG}$.

**Model fitting**

The fitting process was complicated by the spatial and temporal order of caspase 3/7 activation due to the propagation of apoptotic waves. To mitigate this effect, we aligned the trajectories of (Z-DEVD)$_2$-R110 (with respect to time) and defined a relative time (also in units of minutes). We again utilized the two-component Gaussian mixture model fit and established a threshold at which the rhodamine 110 signal was 1000 times more likely to fall within the greater component than the lesser one. All trajectories were aligned to the first time point to pass this threshold, and a time window of 60 min around this time point was selected. The model described above was fitted to the R110 concentration within this time window. For this fitting, we employed the SAEMIX package in R, which is a stochastic approximation-based mixed-effect model approach. The SAEMIX algorithm is more robust and time-efficient than the commonly used nonlinear least square (NLS) algorithm for this purpose.

The mixed-effect model decomposes a "population" of varied observations into a population-level mean effect and individual-level random effects. We reported the population-level $k_C$ and only considered individual-level $k_C$ when demonstrating the individual-level fit. As in wave speed measurements, we calculated medians from observations within the same tube and then from tubes of the same biological replicate. The means and S.E.M.s were reported from all biological replicates.

**List of parameters and variables**

| Name | Meaning | Value | Unit | Source |
|---|---|---|---|---|
| $R(t)$ | Free, fluorescent Rhodamine 110 concentration | | nM | Measured |
| $R_{total}$ | Total concentration of (Z-DEVD)$_2$-R110 and Rhodamine 110 | 2000 | nM | Nominal |
| $R_0$ | Initial concentration of Rhodamine 110 | | nM | Estimated |
| $C(t)$ | Active caspase 3/7 concentration | | nM | Fitted |

| | | | | |
|---|---|---|---|---|
| $C_{total}$ | Total concentration of inactive and active caspase 3/7 | 100 – 400 | nM | Assumed |
| $C_0$ | Initial concentration of active caspase 3/7 | | nM | Fitted |
| $k_R$ | Rate coefficient for (Z-DEVD)$_2$-R110 cleavage by caspase 3/7 | | $nM^{-1}$ $min^{-1}$ | Measured |
| $k_C$ | Rate coefficient for inactive caspase 3/7 activation by active caspase 3/7 | | $nM^{-1}$ $min^{-1}$ | Fitted |
| $k_{BG}$ | Rate coefficient for background nonspecific cleavage of (Z-DEVD)$_2$-R110 | | $min^{-1}$ | Fitted |

## Model fitting for scaling relationships

We fitted a linear model to the log-transformed means of the effective diffusion coefficient, $D_{eff}$, and the rate coefficient, $k_C$. Additionally, we employed the generalized Luther's equation to fit the means of trigger wave speed. In the case of the generalized Luther's equation, fitting was carried out using the NLS algorithm within the stats package in R.

## Acknowledgements

This work was supported by a grant from the NIH (R35 GM131792) to J.E.F. and (K99 GM143481) to W.Y.C.H.

## Author contributions

J.H., Y.C., and J.E.F. conceptualized the study. J.H., Y.C., and S.T. performed the extract experiments. W.Y.C.H. and J.H. performed FCS experiments. J.H., Y. C., and J.E.F. analyzed the data. J.H. and J.E.F. conceptualized the model. J.H. and J.E.F. wrote the manuscript. J.E.F. supervised the study. J.E.F. and W.Y.C.H. secured the funding.

## Declaration of competing interests

The authors declare no competing interests.

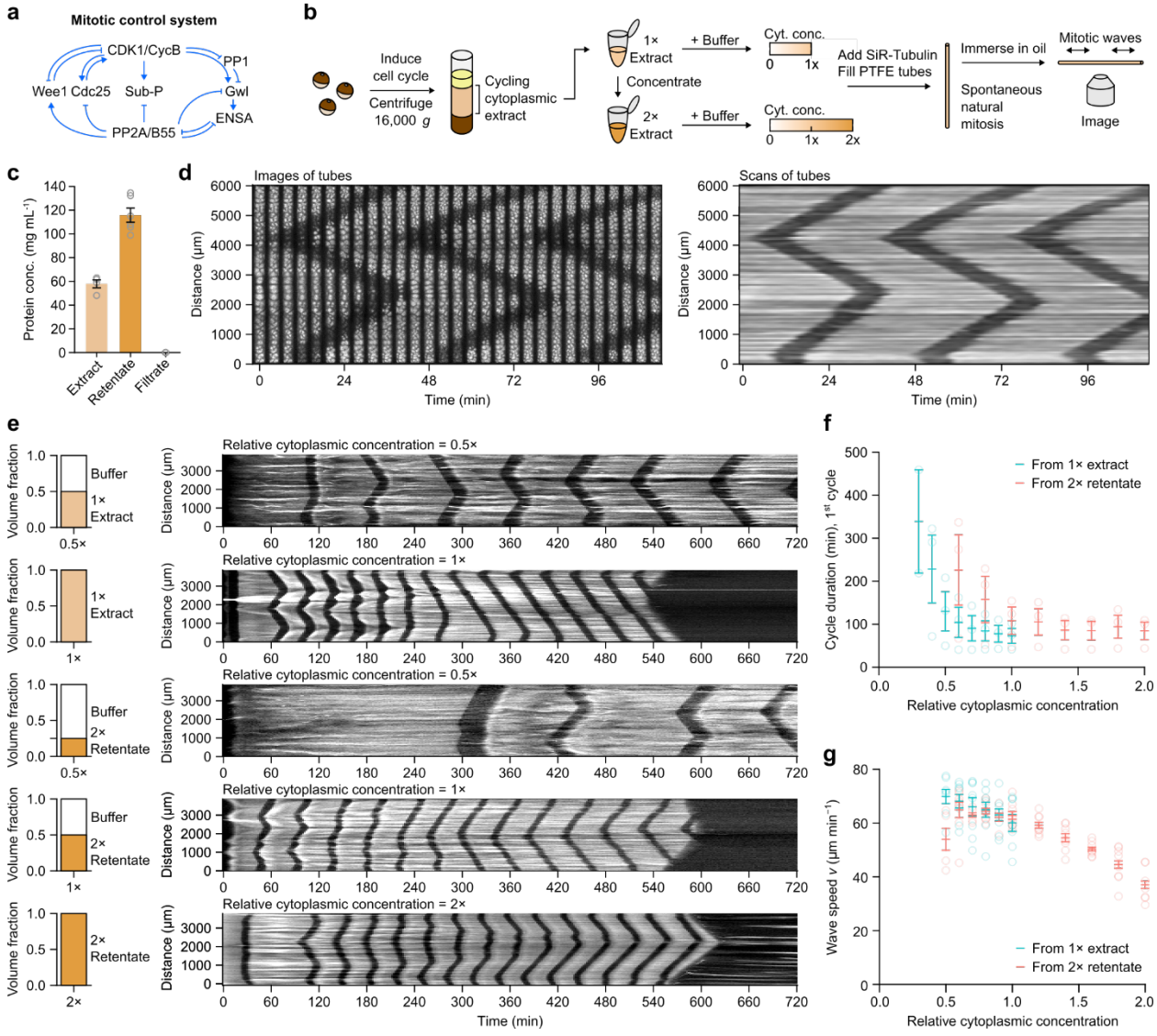


**Figure 1. Mitotic trigger wave speed is robust to change in cytoplasmic concentration.**

**a** Schematic view of the mitotic control network. Note the multiple interconnected positive and double-negative feedback loops. **b** Preparation of cycling *Xenopus* egg extracts and the workflow of monitoring spontaneous mitotic trigger waves in thin PTFE tubes by epifluorescence microscopy. **c** Measurements of protein concentrations in the original and concentrated extract (retentate) as well the filtrate from the ultrafiltration filters. **d** A montage (left) and its corresponding kymograph (right) of a single tube undergoing 3 rounds of mitosis in

741 the course of ~2 hours. The bright signal is polymerized microtubules stained with SiR-tubulin
742 and the dark bands correspond to the mitotic state in which most microtubules are
743 depolymerized. **e** Representative kymographs (right column) of extracts of different
744 cytoplasmic concentrations prepared from 1x extracts (top 2 rows) or from 2x retentate
745 (bottom 3 rows). Left column shows the volume fractions of buffer (XB buffer without sucrose)
746 and extracts that went into the samples. **f** Duration of the first completely observable cell cycle
747 under the microscope, starting from interphase. Means ± S.E.M. are shown, n = 3 (three
748 independent experiments). **g** Speeds of mitotic trigger waves at different cytoplasmic
749 concentrations. Means ± S.E.M. are shown. Data is compiled from 8 independent experiments.
750

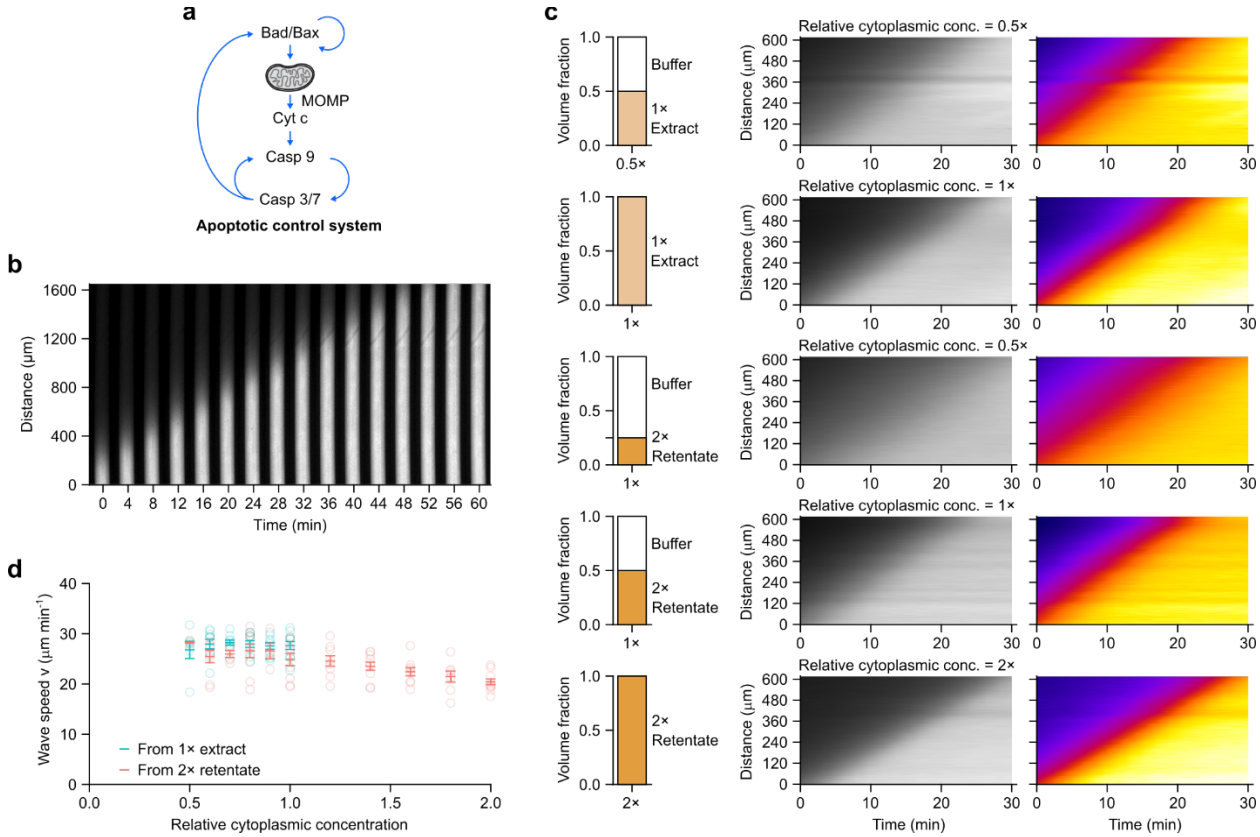


**Figure 2. Apoptotic trigger wave speed is robust to change in cytoplasmic concentration.**

**a** Schematic view of the apoptotic control system. Note the multiple positive feedback loops. **b** A representative montage of an apoptotic trigger wave in a PTFE tube induced from the lower end. Bright signal is rhodamine 110 released by caspase 3/7 cleavage of $(Z\text{-}DEVD)_2$-R110, which reports the activation of caspase 3/7. **c** Representative kymographs (middle and right columns) of extracts at different cytoplasmic concentrations prepared from either 1x extract (top 2 rows) or retentate (bottom 3 rows). Rhodamine 110 fluorescence is shown in grey scale (middle column) or pseudo-color (right column). Pseudo-coloring demonstrates that a range of fluorescence thresholds would give very similar estimates of trigger wave velocity. **d** Speeds of apoptotic trigger waves at different cytoplasmic concentrations. Means ± S.E.M. are shown. Data is compiled from 9 independent experiments.

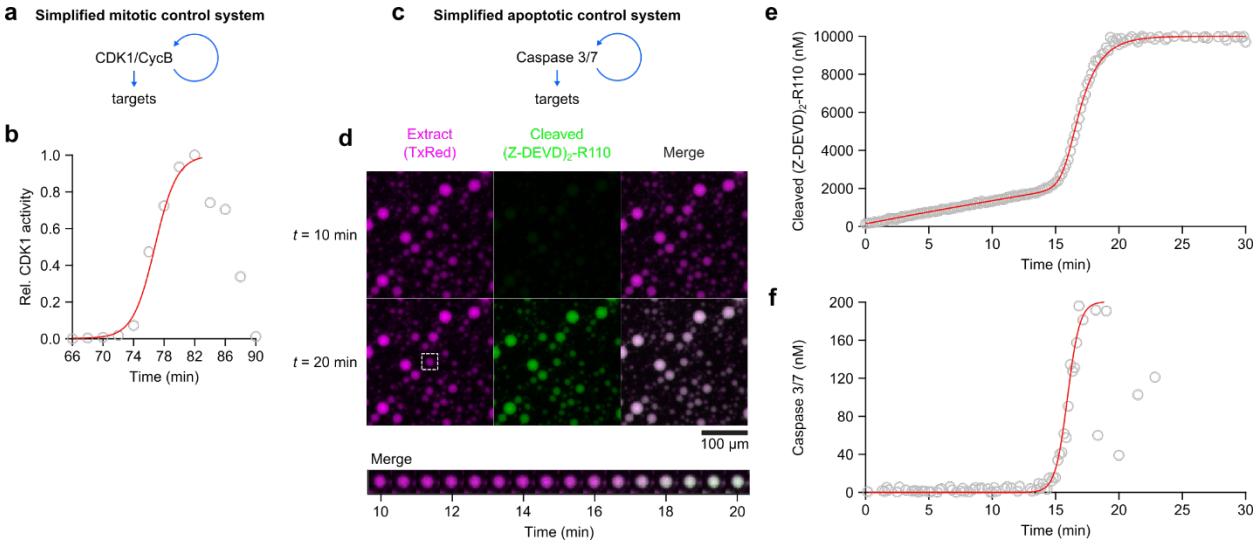


764

765 **Figure 3. Mitotic and apoptotic activities are well-approximate by the logistic equation.**

766 **a** Mitotic control system can be conceptualized more simply as a single, combined positive
767 feedback loop controlling CDK1/CycB at the onset of mitosis. **b** Relative CDK1 activity at mitotic
768 onset, as measured by H1 kinase activity assay, can be well-fitted by a logistic model. Data are
769 taken from Pomerening et al[36]. **c** The apoptotic control system can also be conceptualized as a
770 single, combined positive feedback loop onto caspase 3/7. **d** Apoptosis in droplets of
771 encapsulated extract. Extract containing added $(Z\text{-}DEVD)_2$-R110 plus apoptotic extract and a
772 cytoplasmic marker (TXRed) were encapsulate in squalene plus 5% (v/v) Cithrol DPHS-SO-(AP).
773 Fluorescence was followed as a function of time by microscopy. **e** Kinetics of $(Z\text{-}DEVD)_2$-R110
774 cleavage. Open circles are data at each time point. The red curve is based on the ODE model for
775 caspase 3/7 activation and $(Z\text{-}DEVD)_2$-R110 cleavage (Eqs 9 and 10) fitted to the data. **f** Kinetics
776 of caspase 3/7 activation. Open circles are concentrations of active caspase 3/7 calculated
777 based on the ODE model (Eqs 9 and 10). Red curve is the logistic growth curve fitted to the
778 data.

779

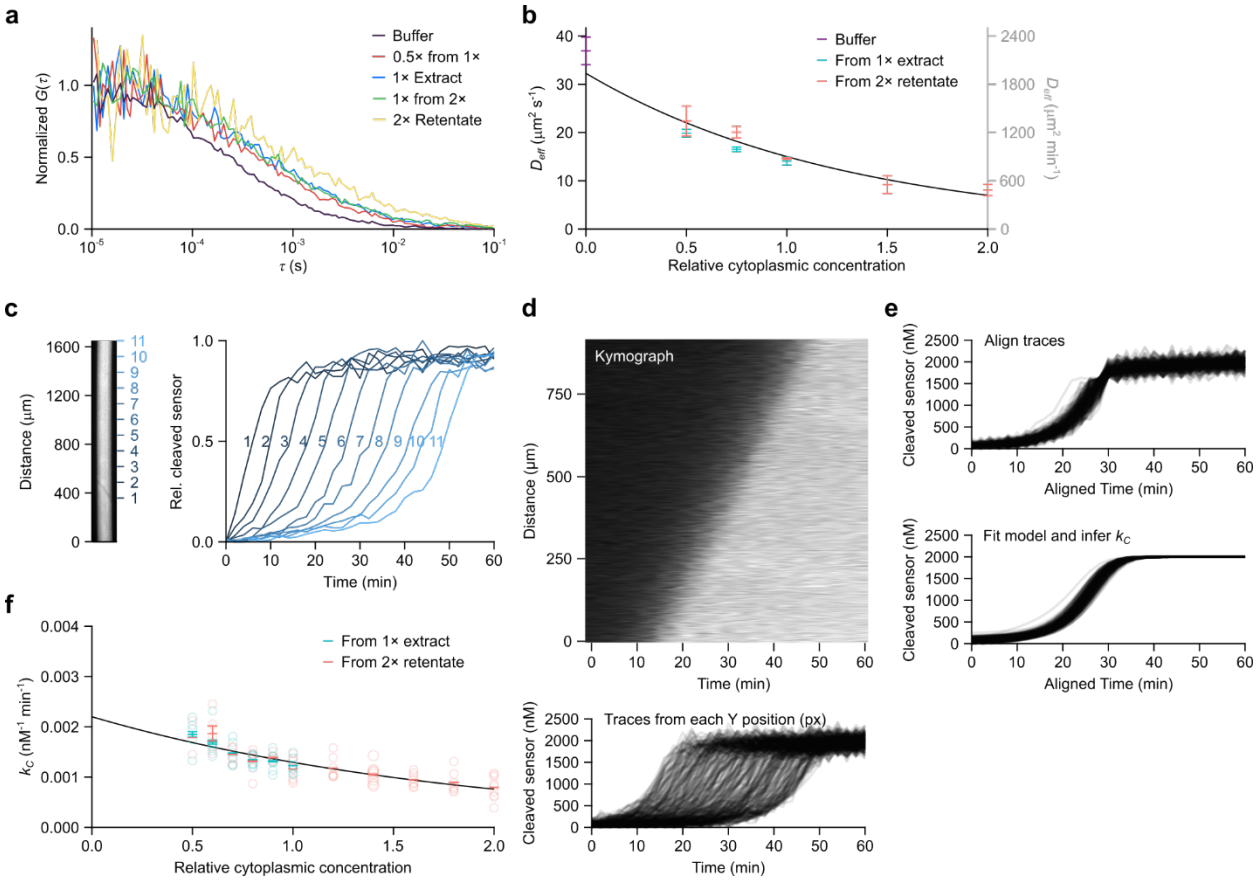


**Figure 4. The effective diffusion coefficient of AF488-BSA and apparent autocatalytic rate constant of caspase 3/7 decrease exponentially with cytoplasmic concentration.**

**a** Representative fluorescence correlation spectroscopy (FCS) autocorrelation functions for AF488-BSA in extracts with different cytoplasmic concentrations. $G(\tau)$ is the autocorrelation function and $\tau$ is the time delay. **b** Effective diffusion coefficient of AF488-BSA at different cytoplasmic concentrations. Effective diffusion coefficients were calculated by fitting the autocorrelation data from FCS measurements to a Brownian diffusion model. A 60 s fluorescence intensity time course was registered for each FCS measurement. Means ± 90% CI calculated from 3 measurements are shown. Solid black curve is an exponential curve fitted to the means. **c** $(Z\text{-DEVD})_2$-R110 cleavage kinetics can be monitored as apoptotic trigger waves sweep through a tube of extract. In this example, fluorescence from cleaved $(Z\text{-DEVD})_2$-R110 at 11 positions (left) are shown on the right. Fluorescence from the cleaved $(Z\text{-DEVD})_2$-R110 was normalized to the maximal value at each location. **d** $(Z\text{-DEVD})_2$-R110 cleavage kinetics in a kymograph (upper) can be represented as a series of traces (lower). **e** Traces shown in (**d**) were

795 aligned by time (upper) and the model for caspase 3/7 activation and (Z-DEVD)$_2$-R110 cleavage
796 was fitted to the data. Individual fitted traces are shown in the bottom panel. **f** The apparent
797 autocatalytic rate constant $k_C$ at different cytoplasmic concentrations was extracted from the
798 fitted model. Shown are means ± S.E.M. compiled from the same 9 experiments as the ones
799 shown in Fig. 2d. The black solid curve is an exponential curve fitted to the means.
800

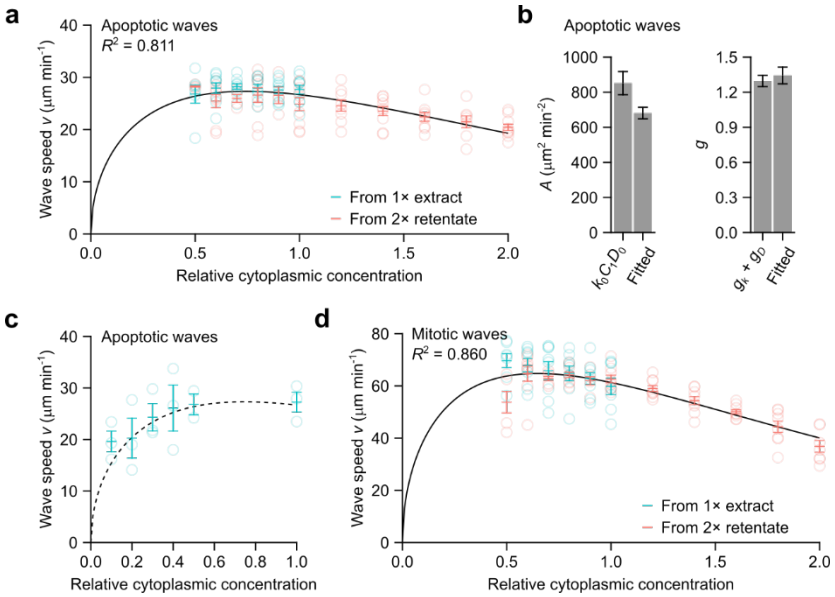


**Figure 5. Mitotic and apoptotic trigger wave speeds at different cytoplasmic concentrations follow the generalized Luther's equation.**

**a** Apoptotic wave speeds at different cytoplasmic concentrations as shown in Fig. 2D. The solid black curve is the generalized Luther's equation fitted to the means. **b** The value of $A$, calculated as the product of the experimentally-determined parameters $k_0$, $D_0$, and $C_1$, is compared to the fitted value (left panel). Likewise, the value of $g$ calculated as the sum of the experimentally-determined parameters $g_k$ and $g_D$, is compared to the fitted value (right panel). $k_0$, $D_0$, $g_k$, and $g_D$ are from the exponential fit shown in Fig. 4. Error bars are S.E.M.s calculated directly from the fittings or propagated from the individual experimentally-determined parameters. **c** Apoptotic wave speeds at low cytoplasmic concentrations. Dashed line shows the same fitted curve as in (**a**), which was obtained from only higher concentration data. Shown are means ± S.E.M. from 3 independent samples. **d** Mitotic wave speeds at different cytoplasmic concentrations, replotted from Fig. 1g and fitted to the generalized Luther's equation (black curve).

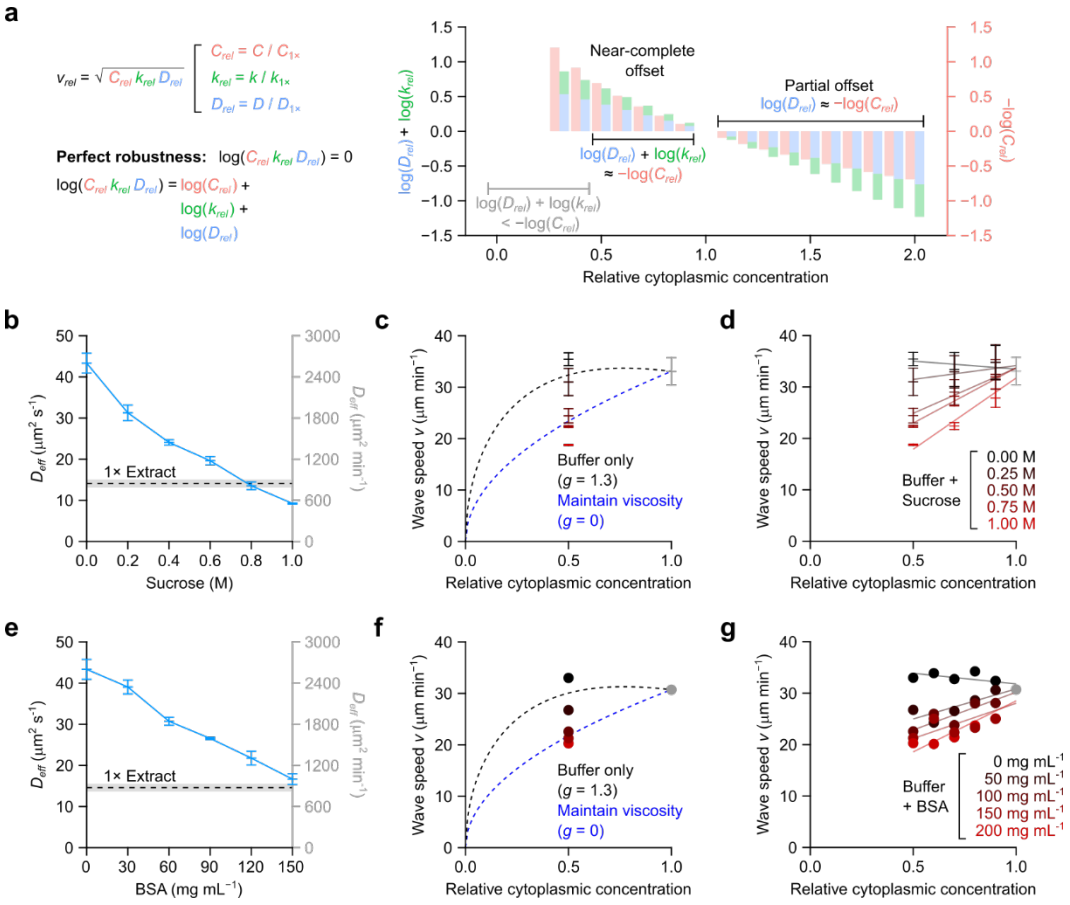


**Figure 6. Opposing kinetic and physical effects give rise to robustness in trigger wave speeds.**

**a** Comparing the effect sizes of changes in rate constant, effective diffusion coefficient, and concentration. Effect size is defined as fold change relative to 1x cytoplasmic concentration. For simplicity, the data for cytoplasmic concentrations < 0.3x, where the concentration effect dominates, are omitted. **b**, **e** Effective diffusion coefficients of AF488-BSA in XB buffers of various sucrose concentrations (**b**; no BSA present) or BSA concentrations (**e**; no sucrose present) as determined by FCS. AF488-BSA diffusion in 1x extract can be mimicked by ~0.8 M sucrose or ~150 mg mL$^{-1}$ BSA. **c**, **f** Apoptotic trigger wave speeds with extracts diluted with buffer (black data points) or a viscogen (red data points), and compared with theoretical curves (dashed lines). Crowding effects are quantified by the parameter $g$. For apoptotic trigger waves, $g$ is ~1.3 (Fig. 5b) and is 0 if crowding effects are absent. We note that, in the case of $g = 0$, wave speed $v$ follows the square root of total caspase 3/7 concentration $\sqrt{C_{rel}}$. Means ± S.E.M. (n = 3) are shown for sucrose-containing buffers (**c**). Means (n = 2) are shown for BSA-containing buffers (**f**). The curves were set to pass through wave speeds at 1x cytoplasmic

concentration for both sucrose-containing and BSA-containing buffers. Apoptotic wave speeds at 0.5x cytoplasmic concentration are also plotted. We note the scaling can be approximated by a horizontal line for $g = 1.3$ between 0.5x and 1x cytoplasmic extract, whereas for $g = 0$, a straight line with a positive slope. **d**, **g** Apoptotic trigger wave speeds are plotted for a range of sucrose-containing (**d**) or BSA-containing buffers (**g**) at different cytoplasmic concentrations. Means ± S.E.M. (n = 3) are shown for sucrose-containing buffers (**d**) whereas means (n = 2) are shown for BSA-containing buffers (**g**). Straight lines were fitted to each sucrose (**d**) or BSA (**g**) concentration. Only buffer without sucrose or BSA manifest straight lines with slightly negative slopes. Viscogen-containing buffers, be it sucrose or BSA, manifest positive slopes.

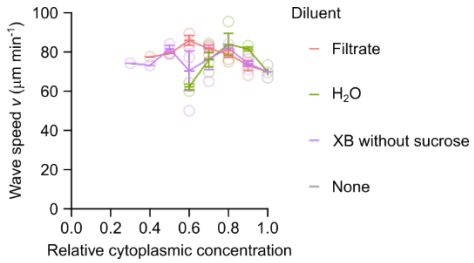


842

843

844 **Supplementary Figure 1, related to Fig. 1. Mitotic trigger wave speed is robust to dilution**

845 **using either filtrate or buffer.**

846 Speeds of mitotic trigger waves at different cytoplasmic concentrations. The cycling extracts

847 were diluted using either filtrate, XB buffer without sucrose, or water. Note that dilution with

848 filtrate and buffer produced comparable wave speeds, whereas dilution with water resulted in

849 a drop in speed. For extracts diluted with water below 0.6x, cycle progression was not

850 observed. Means ± S.E.M. compiled from 3 independent samples are shown.

851

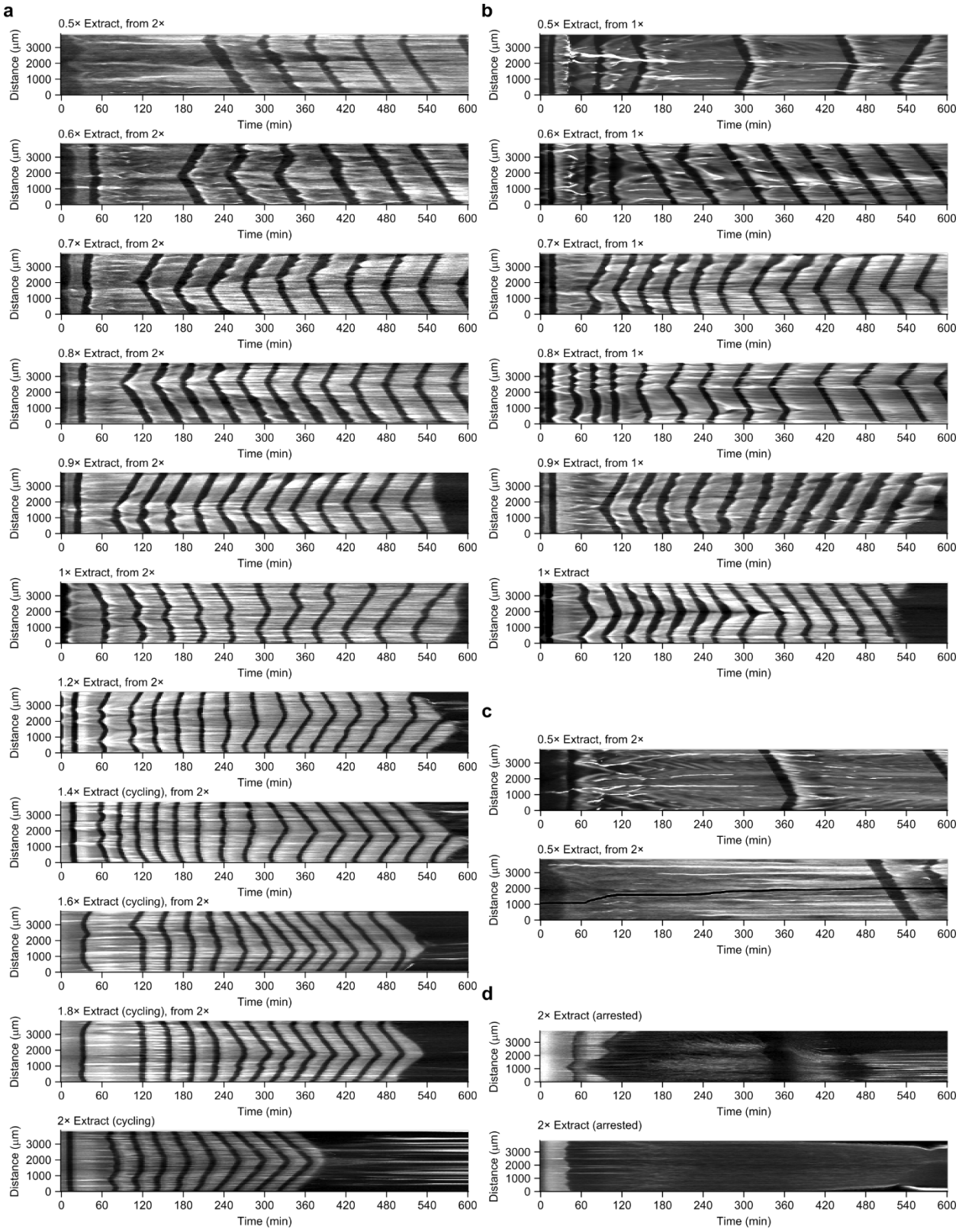

**Supplementary Figure 2, related to Fig. 1. Cell cycle and mitotic trigger waves at different cytoplasmic concentrations.**

**a**, **b** Representative kymographs depict cell cycle and mitotic trigger waves at various cytoplasmic concentrations, prepared from 2x retentate (**a**) and 1x extract (**b**). **c** Two additional instances showcase 0.5x extracts prepared from 2x retentate, highlighting the variability in the first complete cell cycle across different extracts. **d** In contrast to the continuous cycling observed in Fig. 1e, these two examples of 2x retentate underwent mitotic arrest, occurring either in the first mitosis or the second.

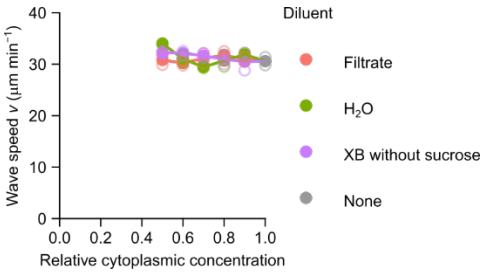


**Supplementary Figure 3, related to Fig. 2. Apoptotic trigger wave speed is robust to dilution using filtrate, buffer, and water.**

Speeds of apoptotic trigger wave at different cytoplasmic concentrations. The interphase extracts were diluted using either filtrate, XB buffer without sucrose, or water. Means from 2 independent samples are shown.

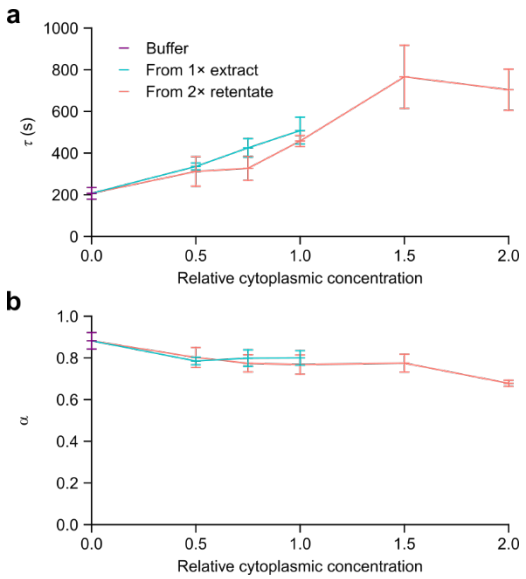


871

872

873 **Supplementary Figure 4, related to Fig. 4. Anomalous diffusion fit to AF488-BSA diffusion in**

874 **extracts.**

875 **a**, **b** FCS autocorrelation functions of AF488-BSA in extracts analyzed using the anomalous

876 diffusion framework. Diffusion time $\tau_D$ (**a**) and anomalous diffusion exponent $\alpha$ (**b**) at different

877 cytoplasmic concentrations.

878

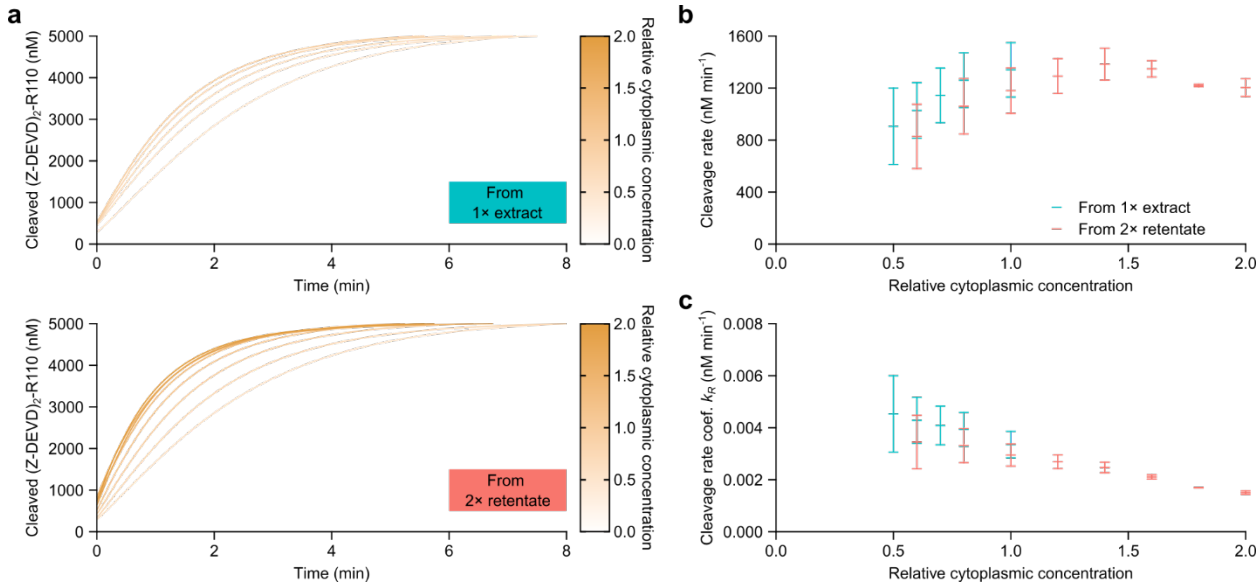


**Supplementary Figure 5, related to Fig. 4. Measuring (Z-DEVD)$_2$-R110 cleavage rate coefficient $k_R$.**

**a** Kinetics of (Z-DEVD)$_2$-R110 cleavage in freshly prepared apoptotic extracts at various cytoplasmic concentration. These extracts were prepared from 1x extract (top) or 2x retentate (bottom). **b** Cleavage rates of (Z-DEVD)$_2$-R110 at different cytoplasmic concentrations were estimated based on the initial timepoints. **c** Second-order rate coefficients at different cytoplasmic concentrations were computed by accounting for (Z-DEVD)$_2$-R110 concentration and nominal active caspase 3/7 concentrations. Means ± S.E.M. compiled from 3 independent samples are shown.

## References

1. Ferrell, J. E., Jr & Machleder, E. M. The biochemical basis of an all-or-none cell fate switch in Xenopus oocytes. Science 280, 895–898 (1998).

2. Murray, A. W. & Kirschner, M. W. Cyclin synthesis drives the early embryonic cell cycle. Nature 339, 275–280 (1989).

3. Newport, J. & Spann, T. Disassembly of the nucleus in mitotic extracts: membrane vesicularization, lamin disassembly, and chromosome condensation are independent processes. Cell 48, 219–230 (1987).

4. Cheng, X. & Ferrell, J. E., Jr. Spontaneous emergence of cell-like organization in Xenopus egg extracts. Science 366, 631–637 (2019).

5. Afanzar, O., Buss, G. K., Stearns, T. & Ferrell, J. E., Jr. The nucleus serves as the pacemaker for the cell cycle. Elife 9, e59989 (2020).

6. Guan, Y. et al. A robust and tunable mitotic oscillator in artificial cells. Elife 7, (2018).

7. Deming, P. & Kornbluth, S. Study of Apoptosis In Vitro Using the Xenopus Egg Extract Reconstitution System. in Xenopus Protocols: Cell Biology and Signal Transduction (ed. Liu, X. J.) 379–393 (Humana Press, 2006).

8. Cheng, X. & Ferrell, J. E., Jr. Apoptosis propagates through the cytoplasm as trigger waves. Science 361, 607–612 (2018).

9. Novak, B. & Tyson, J. J. Modeling the Cell Division Cycle: M-phase Trigger, Oscillations, and Size Control. J. Theor. Biol. 165, 101–134 (1993).

10. Gelens, L., Anderson, G. A. & Ferrell, J. E., Jr. Spatial trigger waves: positive feedback gets you a long way. Mol. Biol. Cell 25, 3486–3493 (2014).

11. Winfree, A. T. Spiral waves of chemical activity. Science 175, 634–636 (1972).

12. Chang, J. B. & Ferrell, J. E., Jr. Mitotic trigger waves and the spatial coordination of the Xenopus cell cycle. Nature 500, 603–607 (2013).

13. Shaffer, B. M. Secretion of cyclic AMP induced by cyclic AMP in the cellular slime mould Dictyostelium discoideum. Nature 255, 549–552 (1975).

14. Robertson, A., Drage, D. J. & Cohen, M. H. Control of Aggregation in Dictyostelium discoideum by an External Periodic Pulse of Cyclic Adenosine Monophosphate. Science 175, 333–335 (1972).

15. Goldbeter, A. & Segel, L. A. Unified mechanism for relay and oscillation of cyclic AMP in Dictyostelium discoideum. Proc. Natl. Acad. Sci. U. S. A. 74, 1543–1547 (1977).

16. De Simone, A. et al. Control of osteoblast regeneration by a train of Erk activity waves. Nature (2021) doi:10.1038/s41586-020-03085-8.

17. Aoki, K. et al. Propagating Wave of ERK Activation Orients Collective Cell Migration. Dev. Cell 43, 305–317.e5 (2017).

18. Fan, Y. et al. Ultrafast distant wound response is essential for whole-body regeneration. Cell 186, 3606–3618.e16 (2023).

19. Takagi, J. & Shimamoto, Y. High-quality frozen extracts of Xenopus laevis eggs reveal size-dependent control of metaphase spindle micromechanics. Mol. Biol. Cell 28, 2170–2177 (2017).

20. Pelletier, J. F., Field, C. M., Coughlin, M. & Ryazanova, L. Glycogen-dependent demixing of frog egg cytoplasm at increased crowding. bioRxiv (2021).

21. Chen, Y., Huang, J.-H., Phong, C. & Ferrell, J. E., Jr. Protein homeostasis from diffusion-dependent control of protein synthesis and degradation. bioRxiv (2023) doi:10.1101/2023.04.24.538146.

22. Liu, X., Oh, S. & Kirschner, M. W. The uniformity and stability of cellular mass density in mammalian cell culture. Front Cell Dev Biol 10, 1017499 (2022).

23. Dill, K. A., Ghosh, K. & Schmit, J. D. Physical limits of cells and proteomes. Proc. Natl. Acad. Sci. U. S. A. 108, 17876–17882 (2011).

24. Zlotek-Zlotkiewicz, E., Monnier, S., Cappello, G., Le Berre, M. & Piel, M. Optical volume and mass measurements show that mammalian cells swell during mitosis. J. Cell Biol. 211, 765–774 (2015).

25. Son, S. et al. Resonant microchannel volume and mass measurements show that suspended cells swell during mitosis. J. Cell Biol. 211, 757–763 (2015).

946 26. Neurohr, G. E. et al. Excessive Cell Growth Causes Cytoplasm Dilution And Contributes to
947 Senescence. Cell 176, 1083–1097.e18 (2019).
948 27. Guo, M. et al. Cell volume change through water efflux impacts cell stiffness and stem
949 cell fate. Proc. Natl. Acad. Sci. U. S. A. 114, E8618–E8627 (2017).
950 28. Venkova, L. et al. A mechano-osmotic feedback couples cell volume to the rate of cell
951 deformation. Elife 11, (2022).
952 29. Nagy, T. L., Strickland, J. & Weiner, O. D. Neutrophils actively swell to potentiate rapid
953 migration. eLife (2023) doi:10.7554/elife.90551.
954 30. Sha, W. et al. Hysteresis drives cell-cycle transitions in Xenopus laevis egg extracts. Proc.
955 Natl. Acad. Sci. U. S. A. 100, 975–980 (2003).
956 31. Pomerening, J. R., Sontag, E. D. & Ferrell, J. E., Jr. Building a cell cycle oscillator:
957 hysteresis and bistability in the activation of Cdc2. Nat. Cell Biol. 5, 346–351 (2003).
958 32. Nolet, F. E. et al. Nuclei determine the spatial origin of mitotic waves. Elife 9, (2020).
959 33. Pacher, P. & Hajnóczky, G. Propagation of the apoptotic signal by mitochondrial waves.
960 EMBO J. 20, 4107–4121 (2001).
961 34. Garcia-Perez, C. et al. Bid-induced mitochondrial membrane permeabilization waves
962 propagated by local reactive oxygen species (ROS) signaling. Proc. Natl. Acad. Sci. U. S. A. 109,
963 4497–4502 (2012).
964 35. Lartigue, L. et al. An intracellular wave of cytochrome c propagates and precedes Bax
965 redistribution during apoptosis. J. Cell Sci. 121, 3515–3523 (2008).
966 36. Pomerening, J. R., Kim, S. Y. & Ferrell, J. E. Systems-Level Dissection of the Cell-Cycle
967 Oscillator: Bypassing Positive Feedback Produces Damped Oscillations. Cell 122, 565–578
968 (2005).
969 37. Good, M. C., Vahey, M. D., Skandarajah, A., Fletcher, D. A. & Heald, R. Cytoplasmic
970 volume modulates spindle size during embryogenesis. Science 342, 856–860 (2013).
971 38. Fisher, R. A. The wave of advance of advantageous genes. Ann. Eugen. 7, 355–369
972 (1937).

973 39. Kolmogorov, A. N., Petrovsky, I. G. & Piskunov, N. S. A study of the diffusion equation
974 with increase in the amount of substance, and its application to a biological problem. in
975 Selected Works of A. N. Kolmogorov 242–270 (Springer Netherlands, 1991).
976 40. Luther, R. Propagation of chemical reactions in space. J. Chem. Educ. 64, 740 (1987).
977 41. Showalter, K. & Tyson, J. J. Luther's 1906 discovery and analysis of chemical waves. J.
978 Chem. Educ. 64, 742 (1987).
979 42. Huang, W. Y. C., Cheng, X. & Ferrell, J. E., Jr. Cytoplasmic organization promotes protein
980 diffusion in Xenopus extracts. Nat. Commun. 13, 5599 (2022).
981 43. Weiss, M., Elsner, M., Kartberg, F. & Nilsson, T. Anomalous subdiffusion is a measure for
982 cytoplasmic crowding in living cells. Biophys. J. 87, 3518–3524 (2004).
983 44. Guigas, G., Kalla, C. & Weiss, M. Probing the nanoscale viscoelasticity of intracellular
984 fluids in living cells. Biophys. J. 93, 316–323 (2007).
985 45. Höfling, F. & Franosch, T. Anomalous transport in the crowded world of biological cells.
986 Rep. Prog. Phys. 76, 046602 (2013).
987 46. Phillies, G. D. J. Universal scaling equation for self-diffusion by macromolecules in
988 solution. Macromolecules 19, 2367–2376 (1986).
989 47. Phillies, G. D. J. Dynamics of polymers in concentrated solutions: the universal scaling
990 equation derived. Macromolecules 20, 558–564 (1987).
991 48. Murray, A. W. Chapter 30 Cell Cycle Extracts. in Methods in Cell Biology (eds. Kay, B. K.
992 & Peng, H. B.) vol. 36 581–605 (Academic Press, 1991).
993 49. Chang, J. B. & Ferrell, J. E., Jr. Robustly Cycling Xenopus laevis Cell-Free Extracts in Teflon
994 Chambers. Cold Spring Harb. Protoc. 2018, (2018).